Ultrafast phosphate hydration dynamics in bulk H_2O

Cite as: J. Chem. Phys. **142**, 212406 (2015); https://doi.org/10.1063/1.4914152
Submitted: 02 December 2014 • Accepted: 23 January 2015 • Published Online: 16 March 2015

Rene Costard, Tobias Tyborski, Benjamin P. Fingerhut, et al.

Ultrafast phosphate hydration dynamics in bulk H_2O

Rene Costard,[a] Tobias Tyborski, Benjamin P. Fingerhut,[b] and Thomas Elsaesser
Max-Born-Institut für Nichtlineare Optik und Kurzzeitspektroskopie, D-12489 Berlin, Germany

(Received 2 December 2014; accepted 23 January 2015; published online 16 March 2015)

Phosphate vibrations serve as local probes of hydrogen bonding and structural fluctuations of hydration shells around ions. Interactions of $H_2PO_4^-$ ions and their aqueous environment are studied combining femtosecond 2D infrared spectroscopy, *ab-initio* calculations, and hybrid quantum-classical molecular dynamics (MD) simulations. Two-dimensional infrared spectra of the symmetric ($\nu_S(PO_2^-)$) and asymmetric ($\nu_{AS}(PO_2^-)$) PO_2^- stretching vibrations display nearly homogeneous lineshapes and pronounced anharmonic couplings between the two modes and with the δ(P-(OH)$_2$) bending modes. The frequency-time correlation function derived from the 2D spectra consists of a predominant 50 fs decay and a weak constant component accounting for a residual inhomogeneous broadening. MD simulations show that the fluctuating electric field of the aqueous environment induces strong fluctuations of the $\nu_S(PO_2^-)$ and $\nu_{AS}(PO_2^-)$ transition frequencies with larger frequency excursions for $\nu_{AS}(PO_2^-)$. The calculated frequency-time correlation function is in good agreement with the experiment. The $\nu(PO_2^-)$ frequencies are mainly determined by polarization contributions induced by electrostatic phosphate-water interactions. $H_2PO_4^-/H_2O$ cluster calculations reveal substantial frequency shifts and mode mixing with increasing hydration. Predicted phosphate-water hydrogen bond (HB) lifetimes have values on the order of 10 ps, substantially longer than water-water HB lifetimes. The ultrafast phosphate-water interactions observed here are in marked contrast to hydration dynamics of phospholipids where a quasi-static inhomogeneous broadening of phosphate vibrations suggests minor structural fluctuations of interfacial water. [http://dx.doi.org/10.1063/1.4914152]

I. INTRODUCTION

Biochemical processes typically involve the interaction of water with specific functional groups of biomolecules.[1] Charged phosphate groups are important units of macromolecules and serve as major hydration sites.[2] The degree and structure of phosphate hydration has a strong influence on the double helix geometry of DNA[3] and on the conformation of phospholipid membranes.[4] Moreover, phosphate ions function as intracellular pH buffers and participate in the metabolism, e.g., the hydrolysis of adenosine triphosphate. While the equilibrium structures of these systems have been well characterized, there is a substantial interest in understanding their dynamics and the underlying molecular interactions. Fluctuations of the hydration structure and vibrational energy relaxation occur on a femto- to picosecond time scale and are relevant for elementary biochemical reactions in living organisms.[5] Understanding these phenomena requires knowledge about the character and dynamics of phosphate-water interactions, in particular hydrogen bonds (HBs), and the interplay of short range fluctuations and long range electrostatics of the charged groups.

Vibrational excitations of water molecules and of functional groups interacting with water molecules are sensitive probes of molecular couplings and structural fluctuations, both being reflected in the vibrational frequencies and lineshapes. Two-dimensional infrared (2D IR) spectroscopy with a femtosecond time resolution allows for mapping molecular dynamics and extracting couplings strengths. Recent 2D IR experiments and theoretical modeling of OH or OD stretch vibrations in neat bulk water,[6–10] at water surfaces,[11,12] in ionic solutions[13–15] as well as in hydration shells of DNA and phospholipids[16–21] have provided detailed insight into the underlying time scales. In the bulk, thermally excited librational motions of H_2O molecules modulate existing HB geometries on a 50 fs time scale. The mean HB lifetime has values of 1-2 ps in the bulk, limited by HB exchange events within 100 fs.[10,22] The role of ions in accelerating or retarding water dynamics has been discussed controversially.[23] 2D IR spectra of water vibrations are spatially unselective, i.e., contain both hydration shell and bulk contributions. A separation of such components, e.g., via different spectral or temporal signatures, has remained difficult.

To map molecular interactions in a spatially selective way, we recently introduced phosphate vibrations as interfacial probes of phosphate-water interactions in hydrated DNA films and phospholipid reverse micelles.[24–26] In phospholipids, the 2D lineshapes of phosphate stretching vibrations display a pronounced inhomogeneous broadening that persists on a time scale on the order of 10 ps and points to minor structural fluctuations of interfacial water.

Here, we apply spatially selective probes for the first time in bulk H_2O and map hydration dynamics of phosphate ions to

[a]costard@mbi-berlin.de
[b]fingerhut@mbi-berlin.de

develop a more general view of phosphate hydration. The 2D infrared spectra of negatively charged $H_2PO_4^-$ ions demonstrate that high-frequency librations of the hydration shell lead to a predominant homogeneous broadening due to frequency modulations on a sub-100 fs time scale. This finding underlines the highly fluctuating nature of the water network around solvated phosphate ions, in marked contrast to the behavior of interfacial water at phospholipids. The experimental results are accounted for by in-depth theoretical calculations of the vibrational structure of hydrated $H_2PO_4^-$ ions and by molecular dynamics (MD) simulations of vibrational dynamics.

The article is organized as follows. In Sec. II, linear vibrational spectra of $H_2PO_4^-$ are analyzed by calculations for $H_2PO_4^-$ embedded in water clusters. The calculated time-averaged hydration structure is presented. Femtosecond pump-probe data for the different $H_2PO_4^-$ vibrations are summarized in Sec. III. The 2D infrared spectra, their analysis by density matrix calculations, and the results of hybrid quantum-classical MD simulations are reported in Sec. IV, concluded by a discussion in Sec. V. Materials and methods are summarized in Sec. VI.

II. VIBRATIONAL SPECTRA AND STRUCTURE OF $H_2PO_4^-$

A 1M solution of KH_2PO_4 (KDP) in H_2O was studied in the experiments. At this concentration, KDP dissociates in K^+ and $H_2PO_4^-$ ions with distinct hydration shells. Fig. 1(a) displays the linear absorption spectrum of a 10 μm thick liquid jet of the solution (solid black line) together with a solvent-subtracted spectrum (solid red line). In accordance

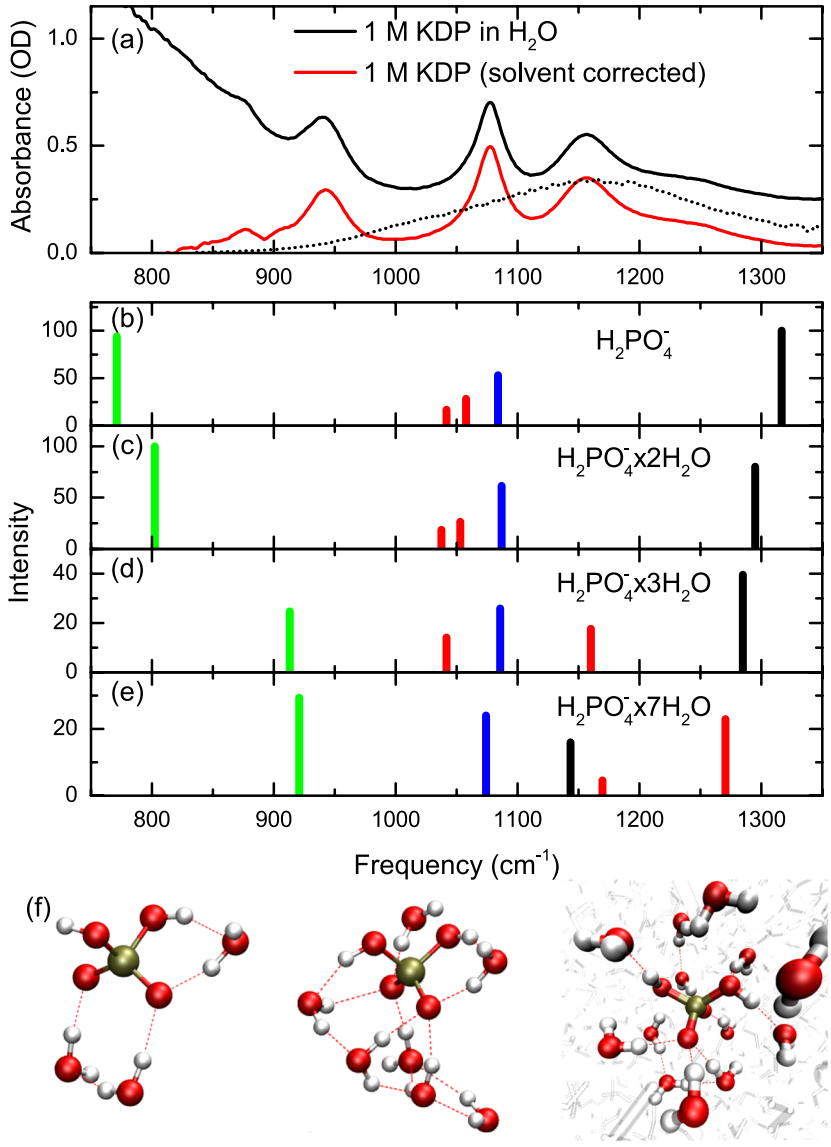

FIG. 1. Vibrational spectra and structure of $H_2PO_4^-$ in aqueous solution. (a) Linear absorption spectrum of a 1M KDP aqueous solution measured in a 10 μm liquid jet (black line) as well as the solvent-corrected absorption (red line). The dotted line shows a typical pulse spectrum used for time-resolved experiments. ((b)-(e)) Frequency positions of $H_2PO_4^-$/water clusters of different sizes obtained by DFT normal mode analysis. The addition of water causes a red shift of $\nu_{AS}(PO_2^-)$ (black) and $\nu_S(PO_2^-)$ (blue) as well as a blue shift of $\nu_{AS}(P—(OH)_2)$ (green) and $\delta(P—(OH)_2)$ (red) resulting in a coupling of $\nu_{AS}(PO_2^-)$ stretching and δ (P—OH) bending modes. (f) Structure of $H_2PO_4^-$ ions hydrated by 3 and 7 water molecules (cf. (d) and (e), respectively) and with a full solvation shell (right, water molecules within 3.5 Å are shown).

with the literature,[27–30] we assign the bands at 880 and 940 cm^{-1} to the symmetric and asymmetric P—$(OH)_2$ stretching vibrations. The bands at 1080 and 1160 cm^{-1} are assigned to the symmetric and asymmetric PO_2^- stretching vibrations ($\nu_S(PO_2^-)$ and $\nu_{AS}(PO_2^-)$) with distinctly different linewidths, and the shoulder around 1250 cm^{-1} to the P—$(OH)_2$ bending vibrations (δ_S (P—$(OH)_2$) and δ_{AS}(P—$(OH)_2$)). The solvent H_2O causes a broad background absorption which is due to the librational L2 band[31] centered at 700 cm^{-1} and a high-frequency librational tail extending up to the OH bending vibration of H_2O at 1650 cm^{-1}.

The vibrational structure of the solute $H_2PO_4^-$ is decisively determined by its interactions with the first water shell, as demonstrated by first-principles normal mode analysis of $H_2PO_4^- \times xH_2O$ clusters ($x = 0 \ldots 7$, Figs. 1(b)–1(f)). Starting from the isolated $H_2PO_4^-$ ion (Fig. 1(b)), the calculated frequency positions hardly match with the experimental linear absorption spectrum in aqueous solution. The asymmetric PO_2^- stretching vibration $\nu_{AS}(PO_2^-)$ appears around 1320 cm^{-1}, followed by the symmetric PO_2^- stretching vibration ($\nu_S(PO_2^-)$ = 1087 cm^{-1}) and the two weak bending modes (δ_{AS}(P—$(OH)_2$) = 1048 cm^{-1} and δ_S(P—$(OH)_2$) = 1031 cm^{-1}). The asymmetric P—$(OH)_2$ stretching vibration (ν_{AS}(P—$(OH)_2$)) appears at 786 cm^{-1} in the gas phase (normal mode displacement vectors of considered modes are depicted in the supplementary material,[32] Fig. S4). Solvation with a discrete number of water molecules at the HB accepting PO_2 positions primarily affects $\nu_{AS}(PO_2^-)$ and ν_{AS}(P—$(OH)_2$) which are shifted by about 20 cm^{-1} towards lower and higher frequency, respectively ($x = 2$, Fig. 1(c)). Further addition of water at the HB donating hydroxyl groups of $H_2PO_4^-$ ($x = 3$, Fig. 1(d)) induces a pronounced blue shift of one of the δ(P—$(OH)_2$) modes and further stabilizes $\nu_{AS}(PO_2^-)$, leading to a delocalization due to mixing of mode character of $\nu_{AS}(PO_2^-)$ and δ(P—$(OH)_2$) normal modes. Upon hydration of all HB binding sites of $H_2PO_4^-$ ($6 \times PO_2 + 2 \times$ P—$(OH)_2$), the observed weak 80 cm^{-1} splitting of the $\nu_S(PO_2^-)$ and $\nu_{AS}(PO_2^-)$ modes is reproduced qualitatively, while both δ(P—$(OH)_2$) modes appear at the highest frequency values ($x = 7$, Figs. 1(e) and 1(f), middle). Accordingly, the bending modes and the asymmetric PO_2^- stretch interchange due to solvation.[29,30] The $\nu_S(PO_2^-)$ mode is only weakly affected by solvation, in agreement with observations on hydrated nucleotides and phospholipids.[24,33] Overall, this cluster analysis underlines that phosphate vibrational frequencies are sensitive probes for ion hydration.

While qualitative agreement in mode assignment and intensities is obtained by the cluster analysis, some differences persist in comparison to the observed vibrational spectrum of KDP in H_2O (Fig. 1(a)). For $x = 7$ (Fig. 1(e)), we find that the frequencies of $\nu_S(PO_2^-)$ and $\nu_{AS}(PO_2^-)$ modes appear slightly below the experimental values already within the employed harmonic approximation. We assign this behavior to an overbinding of $H_2PO_4^-$ with its first solvation shell due to the absence of opposite interactions with a second solvation shell. These deficiencies are resolved in the hybrid quantum-classical description of instantaneous frequency fluctuations used for quantitative comparison with 2D spectra of the $H_2PO_4^-$ (see Sec. IV).

We quantify the microscopic nature of $H_2PO_4^- \cdots H_2O$ HBs by substituting the individual water molecules of the $H_2PO_4^- \times xH_2O$ clusters by point charges followed by normal mode analysis. We find that a quantum mechanical (QM) description of both P—OH coordinated water molecules is necessary to reproduce the vibrational frequencies of the $H_2PO_4^- \times xH_2O$ clusters (entirely treated on QM level). The P—OH coordination mediates mode couplings in the local mode representation and leads to a delocalization of $\nu_{AS}(PO_2^-)$ and δ(P—$(OH)_2$) normal modes determining the vibrational structure of the solute. In contrast, the substitution of PO_2 coordinated water molecules with point charges allows for an accurate calculation of vibrational frequencies of the solvated $H_2PO_4^-$ (for details see supplementary material,[32] Fig. S5). The $\nu(PO_2^-)$ frequencies are thus predominantly determined by polarization contributions and electrostatic interactions while charge transfer contributions are minor.

A. Hydration structure of $H_2PO_4^-$

The time-averaged hydration structure of $H_2PO_4^-$ in aqueous solution is derived from MD simulations of the solute in a cubic box of 1226 water molecules (Fig. 1(f), right). In agreement with the literature,[34,35] we find that the first solvation shell of $H_2PO_4^-$ consists of 12 water molecules, where ≈7.6 water molecules are located at the PO_2 coordination sites and form a tetrahedral environment of the oxygen atoms. Analysis of the P=O$\cdots$O^W radial distribution function (rdf, Fig. 2) reveals that $H_2PO_4^- \cdots H_2O$ distances are slightly reduced compared to bulk water (Δr = 0.06 Å), $H_2PO_4^-$ forms stronger HBs with its surrounding solvent shell.[30,35,36] The structure imposed by $H_2PO_4^-$ on solvent molecules shows a pronounced second maximum in the rdf (5.75 Å) and remaining weak order in the third solvent shell (7.5 Å).

Besides the HB accepting PO_2 functionality, $H_2PO_4^-$ also acts as HB donor via the P—$(OH)_2$ functionality, where HBs are of similar strength. The cluster analysis suggests the presence of bridging water molecules interacting with

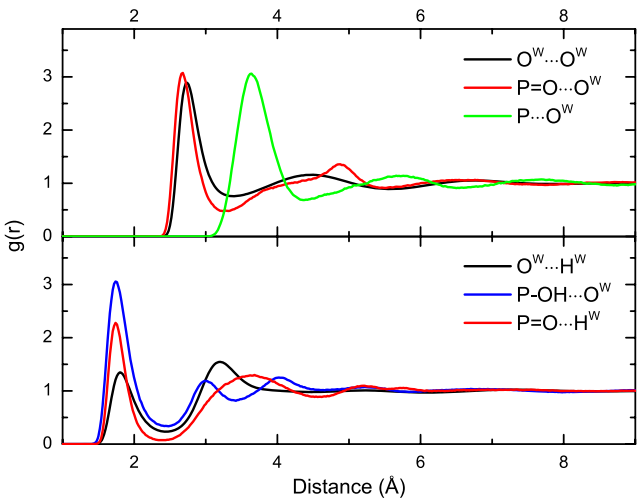

FIG. 2. Oxygen-oxygen and phosphorous-oxygen radial distribution function $g(r)$ as derived from MD simulations (top). Hydrogen-oxygen radial distribution functions $g(r)$ (bottom).

P═O and the P—OH groups simultaneously (Fig. 1(f) left and middle). Such conformations are rarely populated in the MD simulation (Fig. 1(f), right). Instead, we find 3–4 membered rings of water molecules connecting the different P═O and P—OH groups of the phosphate ion leading to a partial alignment of water molecules around the phosphate ion.

Comparison to hydration structures of $H_2PO_4^-$ derived from first principles MD simulations[30,36] shows good agreement in the position of the first maximum and minimum of rdfs, while the population within the first solvation shell appears somewhat higher in the present MD simulations. The higher populations within the first solvation shell of MD simulations, compared to first principles MD, are consistent with previous findings.[37,38]

For the analysis of phosphate-water HBs, we adopt the commonly used geometric definition of the HB[39,40] (oxygen-oxygen distance <3.5 Å, P═O$\cdots$O^W-H^W angle <30°), where the cutoff oxygen-oxygen distance corresponds to the first minimum of the radial distribution function (Fig. 2). On average, the PO_2 coordination sites form a total of 6.5 HBs. Thus, they are the major solvation sites of $H_2PO_4^-$. Further, independent solvation sites are P—OH HB donors (1.9 HBs), while water coordination at P—O^H oxygen atoms is minor ($H_2PO_4^-$ forms a total of 9.7 HBs on average).

HB dynamics and lifetimes are analyzed based on the history independent HB correlation function according to Luzar and Chandler[41] (Fig. S6, supplementary material[32]). The $H_2PO_4^-\cdots H_2O$ HB correlation function is highly non-exponential, where an ultrafast component induced by librational motions (t < 500 fs) is followed by a stretched exponential behavior. The $H_2PO_4^-\cdots H_2O$ HB lifetime τ_{HB} is found to be 10.9 ps, and substantially longer than $H_2O\cdots H_2O$ HB lifetimes.[10,37] For both, the P═O and the P—OH groups, HB lifetimes are similar (Table S3[32]). Interestingly, short time fluctuations lead to a breaking of $H_2PO_4^-\cdots H_2O$ and $H_2O\cdots H_2O$ HBs with similar probability but the separation of contact pairs is slowed down in the Coulomb field of $H_2PO_4^-$ (cf. contact correlation function, Fig. S7, supplementary material[32]).

III. VIBRATIONAL LIFETIMES

The vibrational lifetimes of $\nu_S(PO_2^-)$ and $\nu_{AS}(PO_2^-)$ were determined in femtosecond pump-probe experiments with pump pulses centered around 1140 cm^{-1} (pulse spectrum in Fig. 1(a)). Using the liquid jet sample, we avoid any nonlinear coupling of pump and probe pulses by window materials. In Fig. 3, we summarize (a) pump-probe spectra and (b) time traces taken at different probe frequencies. Excitation by the pump pulse causes a decrease of probe absorption on the fundamental v = 0 → 1 transition by bleaching of the v = 0 ground state and stimulated emission from the v = 1 state. An anharmonically red-shifted absorption arises on the v = 1 → 2 transition of the respective oscillator. This diagonal anharmonicity is estimated from lineshape analysis and vibrational-self-consistent field (vscf) calculations to be on the order of 10 cm^{-1} (Table S2[32]). As is evident from Fig. 3(b), the absorption changes decay nearly completely within 1.5 ps with time constants of 260 ± 20 fs for $\nu_{AS}(PO_2^-)$ and of 345 ± 20 fs for $\nu_S(PO_2^-)$. Such decay times represent

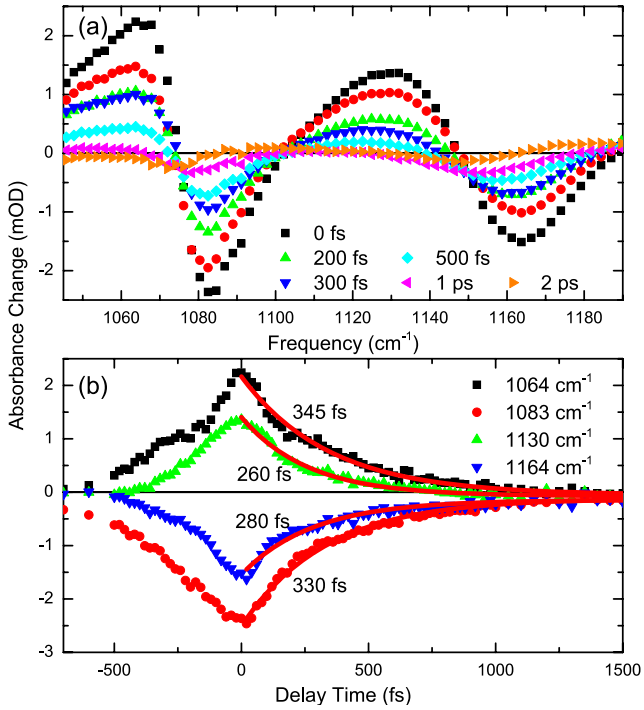

FIG. 3. Pump-probe data of $\nu_S(PO_2^-)$ and $\nu_{AS}(PO_2^-)$. (a) Transient spectra for pump-probe delay times between 0 fs and 2 ps. At early delay times, vibrational excitations cause dispersive signals due to the ground state bleaching and stimulated emission as well as the red-shifted excited state absorption. Energy relaxation heats the system and leads to small thermal signals (T = 2 ps). (b) Time evolution at several fixed probe frequencies (symbols) together with monoexponential fits of the main decay (red lines, time constants). The rise of the signal at negative delay times reflects a perturbed free induction decay.

the v = 1 lifetimes of the oscillators. At negative delay times, the spectrally resolved pump-probe transients in Fig. 3(b) display a finite rise time caused by the so-called perturbed free induction decay.[42] As discussed in the supplementary material,[32] this rise time is consistent with the results obtained from photon echo experiments.

It is instructive to compare the vibrational lifetimes to the values measured for phosphate groups in larger DNA and phospholipid systems.[24–26] Interestingly, there is a universal 300 fs lifetime of $\nu_{AS}(PO_2^-)$ that is independent of the studied system and the water content around the phosphate groups. Such a behavior suggests a common relaxation mechanism that involves low-frequency vibrations of the PO_4 tetrahedron. In contrast, the hydration-dependent lifetime of $\nu_S(PO_2^-)$ in phospholipid model systems is in the range of 1-1.5 ps, a value that clearly exceeds the one measured here.

The phosphate ions are embedded in aqueous solution so that part of the pump pulse is absorbed by water librations which give rise to the background absorption shown in Fig. 1(a). The respective absorbance of water and $H_2PO_4^-$ is proportional to $c_i|\mu_i|^2$, where c_i and μ_i are the respective concentrations and transition dipoles. The water concentration (52M) is much higher than the phosphate concentration (1M), giving a ratio $|\mu_{phosphate}/\mu_{water}|^2 \approx 50$. The respective pump-probe signal scales with $c_i|\mu_i|^4$ and, thus, the water pump-probe signal is negligible compared to the $H_2PO_4^-$ absorption changes. However, relaxation of the $H_2PO_4^-$ stretch

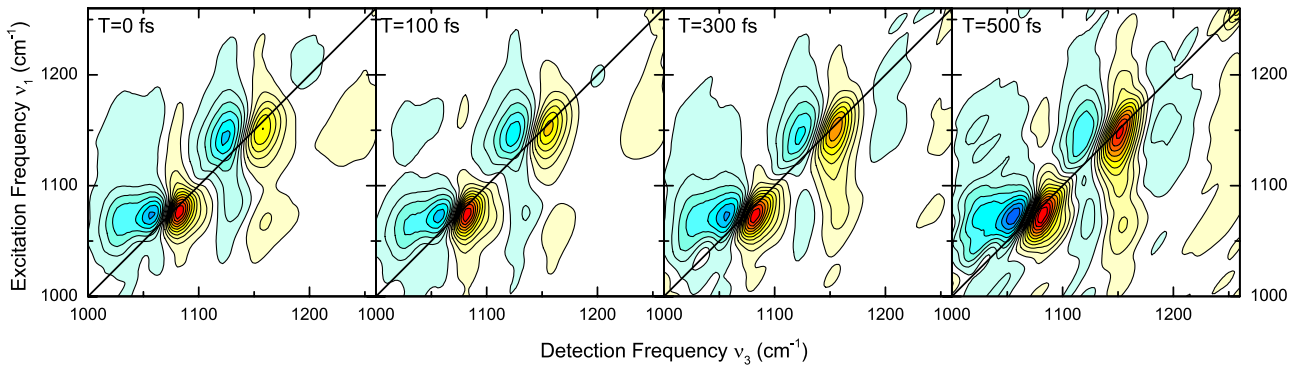

FIG. 4. 2D IR spectra of $H_2PO_4^-$ vibrations for waiting times T between 0 and 500 fs. The normalized absorptive 2D signal is plotted as a function of excitation (ν_1) and detection (ν_3) frequency with an amplitude change of 10% between neighboring contour lines. Yellow-red contours are due to $v = 0 \rightarrow 1$ and blue contours due to $v = 1 \rightarrow 2$ transitions or a thermal signal around $(\nu_1, \nu_3) = (1150, 1190)$ cm^{-1}. Strong pairs of peaks occur at $\nu_1 = 1075$ cm^{-1} ($\nu_S(PO_2^-)$) and $\nu_1 = 1150$ cm^{-1} ($\nu_{AS}(PO_2^-)$). The upright shape of all peaks in the spectra indicates a predominant homogeneous broadening due to fast frequency fluctuations. Off-diagonal cross peaks are due to anharmonic coupling between the different modes.

modes and subsequent energy transfer to the water shell, as well as relaxation of the librations, establish a heated water ground state with a temperature elevated by roughly 1 K. Though small, this temperature rise weakens phosphate-water HBs and leads to thermal blue-shifted pump-probe signals at delay times ≥ 2 ps.

IV. STRUCTURAL DYNAMICS

A. 2D IR spectroscopy

2D spectra of the $H_2PO_4^-$ solution in a spectral range between 1000 and 1250 cm^{-1} are shown in Fig. 4 for different waiting times T. Peaks with yellow-red contours are caused by the $v = 0 \rightarrow 1$ transitions (negative signals in pump-probe spectra), whereas peaks with blue contours are excited state $v = 1 \rightarrow 2$ contributions (positive pump-probe signals). The absorptive 2D signals are normalized to the maximum amplitude of the yellow-red signal to facilitate comparison of the spectral shapes at different T. Intense signals close to the diagonal (excitation frequency ν_1 = detection frequency ν_3) originate from a single vibration and provide information about the line broadening mechanisms, while off-diagonal peaks give insight into couplings between different vibrations.

The 2D spectra in Fig. 4 are dominated by the diagonal peaks of $\nu_S(PO_2^-)$ and $\nu_{AS}(PO_2^-)$ centered at $\nu_1 = 1075$ and 1150 cm^{-1}. In contrast, the signals from δ(P—(OH)$_2$) are weak due to their smaller transition dipole moment. All diagonal peaks show fairly round, homogeneous lineshapes with a small tilt that persists up to T = 500 fs. Strong off-diagonal cross peaks between $\nu_S(PO_2^-)$ and $\nu_{AS}(PO_2^-)$ suggest pronounced vibrational couplings between the stretching vibrations of the $H_2PO_4^-$ ion. In fact, cross peaks also exist between the PO_2^- stretching and the P—(OH)$_2$ bending modes as evident, e.g., from the feature at $(\nu_1, \nu_3) = (1150, 1240)$ cm^{-1}. Further cross peaks are found between $\nu_S(PO_2^-)$ and δ(P—(OH)$_2$); however, they are too weak to be displayed by the lowest contour corresponding to 10% of the maximum signal. A detailed account of vibrational couplings will be given elsewhere. The rising feature at $(\nu_1, \nu_3) = (1150, 1190)$ cm^{-1} (blue, $T > 300$ fs) is assigned to a thermal frequency shift of $\nu_{AS}(PO_2^-)$.

We now discuss the lineshapes of the diagonal peaks. Their upright shape with a small tilt relative to the ν_1 axis clearly points to a predominant homogeneous broadening. This impression is supported by a selection of slices parallel to the frequency diagonal $\nu_1 = \nu_3$ and along a line parallel to the ν_3-axis (horizontal cuts) as summarized in Fig. 5 (symbols). There, the homogeneity is reflected in similar spectral widths of horizontal and diagonal cuts.

To extract the fluctuation amplitudes of the $H_2PO_4^-$ vibrational frequencies and correlation times of the water environment, quantities not directly accessible from the measured

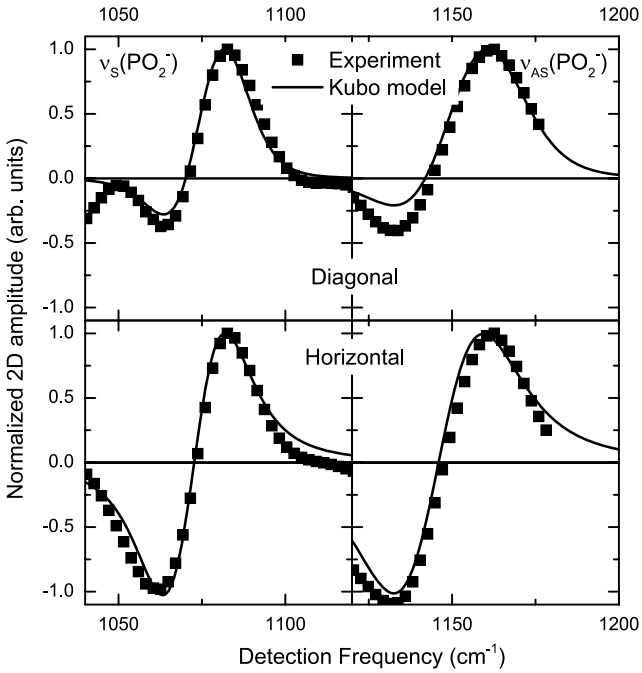

FIG. 5. Experimental (symbols) and calculated (lines) slices through the 2D spectra. The top row shows cuts parallel to the diagonal $\nu_1 = \nu_3$ through the maximum of the fundamental $v = 0 \rightarrow 1$ transitions (waiting time $T = 0$ fs), whereas the bottom row shows horizontal cuts at $\nu_1 = 1080$ cm^{-1} for $\nu_S(PO_2^-)$ and at $\nu_1 = 1155$ cm^{-1} for $\nu_{AS}(PO_2^-)$ ($T = 0$ fs).

2D spectra, we calculate 2D spectra using density matrix theory[43,44] and the response functions detailed in Ref. 26. This approach considers dephasing of vibrational polarizations due to frequency fluctuations and takes into account broadening by the finite vibrational lifetimes. Frequency fluctuations $\delta\nu(t)$ around an average frequency are described by the time correlation function $C(t) = \langle\delta\nu(t)\delta\nu(0)\rangle$, where $\langle\rangle$ denotes the ensemble average. Assuming Gaussian fluctuations (second-order cumulant expansion), the time correlation function of frequency fluctuations is approximated by the biexponential Kubo function,

$$C(t) = (\delta\nu_1)^2 e^{-t/\tau_{C1}} + (\delta\nu_2)^2 e^{-t/\tau_{C2}}, \quad (1)$$

with the fluctuation amplitudes $\delta\nu_{1,2}$ and the underlying correlation times $\tau_{C1,2}$.

The calculated spectra were fitted to the experimental data by comparing spectral slices (cf. Fig. 5) and observing the overall 2D lineshapes (Figs. 6(a) and 6(b)). A good agreement was found by using values of $\approx$10 cm^{-1} for the diagonal anharmonicity (cf. Table S2[32]) and a Kubo function composed of an ultrafast and a static term (cf. Fig. S2),

$$C(t) = (\delta\nu_1)^2 e^{-t/\tau_{C1}} + (\delta\nu_2)^2. \quad (2)$$

We find a common first correlation time τ_{C1} = 50 fs and fluctuation amplitudes $\delta\nu_1$ = 15/27 cm^{-1} for $\nu_S(PO_2^-)/\nu_{AS}(PO_2^-)$. This component represents rapid frequency fluctuations

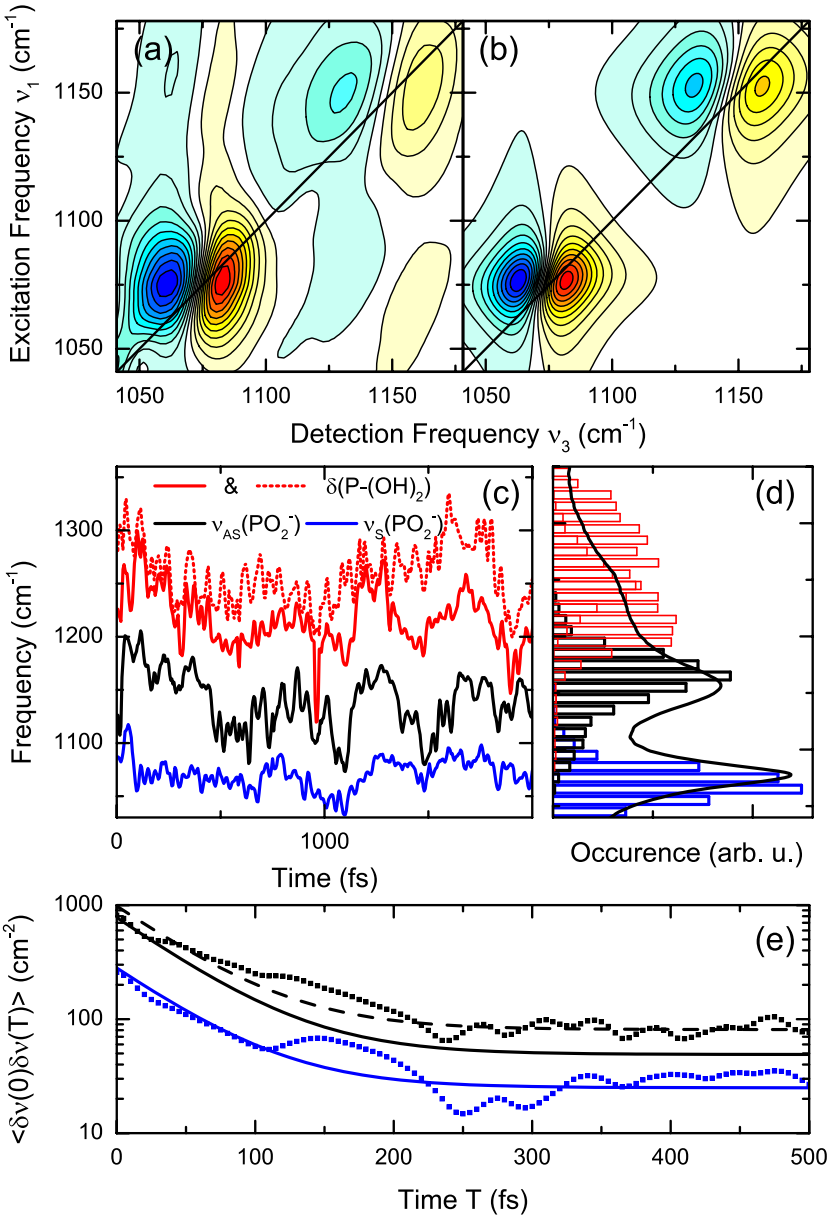

FIG. 6. Structural fluctuations derived from 2D IR spectra and MD simulations. (a) Experimental 2D spectrum of the PO_2 stretching modes $\nu_S(PO_2^-)$ and $\nu_{AS}(PO_2^-)$ at a delay time T = 0 fs. (b) Simulated 2D spectrum of $\nu_S(PO_2^-)$ and $\nu_{AS}(PO_2^-)$; the parameters of the used biexponential Kubo function are $\delta\nu_1 = 15/27$ cm^{-1}, $\delta\nu_2 = 5/7$ cm^{-1}, for $\nu_S(PO_2^-)/\nu_{AS}(PO_2^-)$ and consistent correlation times of $\tau_{C1} = 50$ fs and $\tau_{C2} \to \infty$. (c) Time evolution of instantaneous frequencies in the mixed quantuclassical model. (d) Histogram of frequency distribution calculated at the B3LYP/6-311++G(d,p) density functional level superimposed with the experimental linear absorption spectrum. (e) Frequency-frequency fluctuation correlation function $\langle\delta\nu(0)\delta\nu(T)\rangle$ of $\nu_S(PO_2^-)$ and $\nu_{AS}(PO_2^-)$ modes calculated with the Kubo model and on the density functional level. The symbols and solid lines represent results from the mixed quantum-classical model and the density matrix analysis of 2D spectra, respectively. Dashed line: slightly modified Kubo function with $\delta\nu_1 = 30$cm^{-1}, $\tau_{C1} = 50$ fs and $\delta\nu_2 = 9$ cm^{-1}, $\tau_{C2} = \infty$.

and results in the observed dominantly homogeneously broadened lineshapes. The second component with $\delta\nu_2 = 5/7\ \mathrm{cm}^{-1}$ ($\tau_{C2} \rightarrow \infty$) reflects a minor longer-lived memory of the transition frequency during our observation window $T \leq 500$ fs, indicative for a small contribution of inhomogeneous broadening.

For $\nu_{AS}(PO_2^-)$, the amplitude of the calculated diagonal slices deviates slightly from the experimental results in the red part of the spectrum. In contrast, the amplitudes are well fit for the horizontal slices. We attribute this behavior to the contribution of the cross peaks to the diagonal slices due to the elongation of the experimental 2D spectra along the excitation frequency axis. This elongation is in part induced by overlap effects of diagonal peaks and cross peaks. Additionally, theoretical assumptions such as Gaussian frequency fluctuations used for the second-order cumulant expansion impose limits on the accuracy of the calculations.

As pointed out before, the experimental conditions lead to a resonant excitation of librational modes that could, in principle, contribute to the observed frequency fluctuations. For our pulse energies, however, we excite a fraction of 10^{-3} water molecules at random sites in the liquid. This value is much smaller than the thermal occupation probability of $e^{-1000/200} \approx 7 \times 10^{-3}$ so that we can neglect contributions of resonantly excited librations to the observed frequency fluctuations.

B. Hybrid quantum-classical instantaneous frequency fluctuations

In order to provide microscopic insight into the fastest frequency fluctuations revealed by lineshape analysis of 2D spectra, we analyze the instantaneous frequency fluctuations of $\nu_S(PO_2^-)$, $\nu_{AS}(PO_2^-)$, and $\delta(P—(OH)_2)$ modes along the nuclear configurations generated by a classical MD trajectory. Here, we treat the solute $H_2PO_4^-$ and the two P—OH coordinated H_2O molecules on density functional (DF) level of theory and evaluate the relaxed instantaneous normal modes within the point charge field generated by the surrounding water network (for details see Sec. VI).

A representative time evolution of frequencies within the first 2 ps is shown in Fig. 6(c). Both PO_2^- stretching vibrations $\nu_S(PO_2^-)$ and $\nu_{AS}(PO_2^-)$ fluctuate on an ultrafast 50 fs time scale due to the field fluctuations induced by the HB environment. Fig. 6(d) presents the frequency distribution (without weighting with the intensity of the normal modes) due to solvent induced configurations over the total simulation time of 12 ps ($\Delta t = 5$ fs) superimposed with the linear absorption spectrum (cf. Fig. 1(a)). Frequency fluctuations are least pronounced for $\nu_S(PO_2^-)$, whereas they are stronger for $\nu_{AS}(PO_2^-)$ and the strongest for the $\delta(P—(OH)_2)$ modes. While a direct comparison of (weighted) frequency fluctuations with the linear absorption spectrum is not possible due to the neglect of non-Condon and motional narrowing effects,[45] the calculated mean frequencies of $\nu_S(PO_2^-)$ (1069 cm^{-1}) and $\nu_{AS}(PO_2^-)$ (1158 cm^{-1}) are in very good agreement with the experimental values.

Although the time scale of fluctuations is nearly identical for the two PO_2^- stretching modes, the fluctuation bandwidth $\sigma(\nu_{AS}(PO_2^-)) = 29\ \mathrm{cm}^{-1}$ is substantially larger than $\sigma(\nu_S(PO_2^-)) = 16\ \mathrm{cm}^{-1}$, confirming the high sensitivity of $\nu_{AS}(PO_2^-)$ to local electric fields.[33] Both distributions approximately resemble a Gaussian fluctuation profile (cf. Fig. S3, supplementary material[32]) in the lineshape analysis of the experimental 2D spectra. While the PO_2^- oxygen atoms are HB acceptors, the P—OH hydrogen atoms serve as HB donors to the surrounding water network. The fluctuation bandwidth of both $\delta(P—(OH)_2)$ modes (solid and dashed red lines in Fig. 6(c)) is broad and unstructured and strongly overlaps with the $\nu_{AS}(PO_2^-)$ fluctuation distribution. The larger fluctuation amplitudes of $\nu_{AS}(PO_2^-)$ compared to $\nu_S(PO_2^-)$ are assigned to the mixing with $\delta(P—(OH)_2)$ that exhibits the largest fluctuation amplitude and is correlated with $\nu_{AS}(PO_2^-)$ (cf. Fig. 6(c)). While $\nu_S(PO_2^-)$ selectively probes fluctuations at the PO_2 site, $\nu_{AS}(PO_2^-)$ is additionally sensitive to dynamics of the P—OH HB donors, due to the mode coupling with $\delta(P—(OH)_2)$.

For comparison of time scales observed in 2D spectra and simulations, we calculate the time correlation function of frequency fluctuations $\langle\delta\nu(T)\delta\nu(0)\rangle$ for $\nu_S(PO_2^-)$ and $\nu_{AS}(PO_2^-)$ modes directly from the instantaneous frequencies of the trajectory. For $\nu_S(PO_2^-)$ (Fig. 6(e), blue), we find that both the fluctuation time scale and bandwidth $\langle\delta\nu(0)^2\rangle$ agree well between the Kubo model and the mixed quantum-classical derived frequency fluctuations. For $T \leq 100$ fs, the correlation function decays exponentially and the initial correlation reduces by about 80%. At $T = 150$ fs, we observe a recurrence in the quantum-classical derived frequency correlations, pointing to underdamped low-frequency motions in the coupled system.[7,46]

For $\nu_{AS}(PO_2^-)$ (Fig. 6(e), black), there is less agreement between experiment and theory. However, increasing the amplitudes of the fast and slow Kubo contributions by 3 and 2 cm^{-1} (dashed line in Fig. 6(e)) leads to a similar agreement as for $\nu_S(PO_2^-)$. Such variations of the fluctuation amplitudes are definitely within our experimental accuracy.

V. DISCUSSION

2D IR spectroscopy of the water stretching vibration revealed a rapid 50 fs component of frequency fluctuations originating from thermally excited high-frequency librations.[6–8] Due to the long-range character of the fluctuating electric force and the strong phosphate-water HBs, such librational modes have a strong impact on the hydrated $H_2PO_4^-$ ions. Our present results show for the first time that such ultrafast structural fluctuations determine the lineshapes of both linear absorption and 2D spectra of phosphate vibrations and underline the highly dynamic nature of the hydration shell in bulk water. Despite their limited anharmonicity on the order of 10 cm^{-1}, the PO_2^- stretching vibrations are sensitive probes for structural fluctuations of the hydration shell.

The results presented here are in strong contrast to the lineshapes of phosphate vibrations in phospholipid model systems that are dominantly inhomogeneously broadened.[26] The phospholipid-water interface is subject to very strong electrostatic fields originating from the phosphate-choline dipole moments of approximately 20 D. Such fields have a strong in-plane component at the interface and orient the much smaller water dipoles. Molecular dynamics simulations found

that water molecules connect different phospholipids and that the lifetime of these water bridges is up to 50 ps.[47] Thus, the water shell around phosphate groups in phospholipids is comparably rigid and fluctuating molecular motions to a substantial extent suppressed. Moreover, due to the tilt of phospholipid head groups, this hydration shell water is partly shielded from the surrounding bulk, i.e., the electric force exerted by bulk water fluctuations on both interfacial water and PO_2^- oscillators is much weaker than the dipole forces originating from the head groups. The frequency-time correlation function reported in Ref. 26. (Fig. S2[32]) displays an initial 300 fs decay due to restricted water dynamics and motions of the phospholipid and a pronounced constant component originating from the essentially static structural inhomogeneity of the interface. In contrast, the $H_2PO_4^-$ ions in bulk H_2O are fully exposed to the fluctuating electric field exerted by the water molecules in the first and the outer hydration shells. This leads to fluctuation amplitudes that are 2–3 times larger than in the phospholipid system with the consistent result that the asymmetric phosphate stretching vibration is more sensitive to fluctuations than the symmetric one.

The correlation times apparent from the 2D spectra and the mixed quantum-classical derived frequency calculations are well below the picosecond HB lifetimes reported here and in the literature,[14,22] i.e., we are able to discern sub-100 fs structural fluctuations from slower hydrogen bond exchange dynamics. Owing to the short vibrational lifetimes of 300 fs, these exchange processes do not contribute significantly to the observed 2D line shapes. The MD trajectories suggest a characteristic 10 ps lifetime of a single HB. Consequently, about one phosphate-water HB per 1.5 ps is exchanged at the PO_2 group. While different HB coordination numbers could contribute to the observed inhomogeneity of the phosphate bands and potentially cause the minor reshaping of the 2D spectra at T = 500 fs, further structural analysis is needed to determine contributions to the inhomogeneous linewidth. For example, cis and trans isomers of the $H_2PO_4^-$ hydroxyl groups interchange several times during our MD trajectory representing another possible mechanism for inhomogeneous broadening.

In conclusion, the experimental and theoretical results presented here underline the strong potential of local ionic vibrators for probing ultrafast structural dynamics of aqueous systems and the underlying interactions in a specific way. This concept is not limited to phosphate ions but can be extended to other polyatomic ions in aqueous environment such as sulfate or perchlorate and to functional groups of hydrated biomolecules.

VI. MATERIALS AND METHODS

A. Experimental

The experimental 2D IR setup has been described in detail elsewhere.[6,26] Briefly, tunable mid-IR pulses with a center frequency between 1000 and 1300 cm^{-1}, a spectral bandwidth of 200 cm^{-1}, and a duration of 100 fs are generated by nonlinear parametric frequency conversion.[48] 2D spectra are acquired with a noncollinear 3-pulse photon echo experiment. Amplitude and phase of the nonlinear signal as a function of the coherence time τ and population time T (time delay between the first and second and third pulse, respectively) are measured by heterodyne detection with a weak local oscillator pulse that is dispersed on a 64-pixel MCT detector array (spectral resolution 2 cm^{-1}). The excitation frequency axis is obtained by a Fourier transform along τ. A 1M solution of KDP (>99%, Alfa Aesar) was prepared with distilled water. In order to avoid nonresonant window signals, the sample was held as a gravity-driven liquid jet.[49] Smooth thin films with 10 μm thickness were obtained by adding 6 mM of the surfactant Igepal® CO-890 which left the absorption spectra unchanged. All experiments were performed at room temperature and with linear parallel polarization of the pulses.

B. Simulations

1. Normal mode analysis

First principles calculations of $H_2PO_4^- \times xH_2O$ clusters employed the hybrid exchange correlation DF PBE0 with a 6-311++G(d,p) basis set (an assessment of functionals is given in the supplementary material[32]).

2. MD trajectory calculations

MD simulations were performed, using the Charmm27 all atom force field and the TIP5P water model (cubic box of 1226 water molecules). After equilibration, simulations were performed at constant temperature T = 298 K with a time step of 0.5 fs and saved every 5 fs.

3. Hybrid quantum-classical simulation protocol

Instantaneous frequencies of $H_2PO_4^-$ were calculated along successive configurations of the classical MD trajectory. The solute $H_2PO_4^-$ and two P—OH coordinated H_2O molecules are treated on hybrid DF(B3LYP) level of theory (basis: 6-311++G(d,p), cf. supplementary material[32]), in the field of point charges of all remaining water molecules. Relaxed instantaneous normal modes (rINM) are evaluated by initially optimizing the $H_2PO_4^- \times 2H_2O$ QM region and subsequent normal mode analysis. Geometry optimization prior to the INM Ansatz guarantees the separation of intramolecular fluctuations from solvent induced fluctuations.

ACKNOWLEDGMENTS

The research leading to these results has received funding from the European Research Council under the European Union's Seventh Framework Programme (Grant No. FP7/2007-2013)/ERC Grant. Agreement No. 247051. B.P.F. gratefully acknowledges support through the German Research Foundation (DFG) within the Emmy Noether Programme (Grant No. FI 2034/1-1).

[1]P. Ball, Chem. Rev. **108**, 74 (2008).
[2]F. Westheimer, Science **235**, 1173 (1987).
[3]W. Saenger, W. N. Hunter, and O. Kennard, Nature **324**, 385 (1986).
[4]H. Hauser, I. Pascher, R. Pearson, and S. Sundell, Biochim. Biophys. Acta **650**, 21 (1981).

[5]A. C. Fogarty, E. Duboue-Dijon, F. Sterpone, J. T. Hynes, and D. Laage, Chem. Soc. Rev. **42**, 5672 (2013).
[6]M. L. Cowan, B. D. Bruner, N. Huse, J. R. Dwyer, B. Chugh, E. T. J. Nibbering, T. Elsaesser, and R. J. D. Miller, Nature **434**, 199 (2005).
[7]J. J. Loparo, S. T. Roberts, and A. Tokmakoff, J. Chem. Phys. **125**, 194521 (2006).
[8]J. B. Asbury, T. Steinel, K. Kwak, S. A. Corcelli, C. P. Lawrence, J. L. Skinner, and M. D. Fayer, J. Chem. Phys. **121**, 12431 (2004).
[9]C. P. Lawrence and J. L. Skinner, J. Chem. Phys. **118**, 264 (2003).
[10]D. Laage and J. T. Hynes, Science **311**, 832 (2006).
[11]J. Bredenbeck, A. Ghosh, H.-K. Nienhuys, and M. Bonn, Acc. Chem. Res. **42**, 1332 (2009).
[12]P. C. Singh, S. Nihonyanagi, S. Yamaguchi, and T. Tahara, J. Chem. Phys. **137**, 094706 (2012).
[13]S. Park and M. D. Fayer, Proc. Natl. Acad. Sci. U. S. A. **104**, 16731 (2007).
[14]M. Ji, M. Odelius, and K. J. Gaffney, Science **328**, 1003 (2010).
[15]A. A. Bakulin, M. S. Pshenichnikov, H. J. Bakker, and C. Petersen, J. Phys. Chem. A **115**, 1821 (2011).
[16]M. Yang, Ł. Szyc, and T. Elsaesser, J. Phys. Chem. B **115**, 13093 (2011).
[17]S. Pal, P. K. Maiti, B. Bagchi, and J. T. Hynes, J. Phys. Chem. B **110**, 26396 (2006).
[18]S. Pal, P. K. Maiti, and B. Bagchi, J. Chem. Phys. **125**, 234903 (2006).
[19]K. E. Furse and S. A. Corcelli, J. Am. Chem. Soc. **130**, 13103 (2008).
[20]W. Zhao, D. E. Moilanen, E. E. Fenn, and M. D. Fayer, J. Am. Chem. Soc. **130**, 13927 (2008).
[21]R. Costard, C. Greve, I. A. Heisler, and T. Elsaesser, J. Phys. Chem. Lett. **3**, 3646 (2012).
[22]D. Laage and J. T. Hynes, Proc. Natl. Acad. Sci. U. S. A. **104**, 11167 (2007).
[23]G. Stirnemann, E. Wernersson, P. Jungwirth, and D. Laage, J. Am. Chem. Soc. **135**, 11824 (2013).
[24]Ł. Szyc, M. Yang, and T. Elsaesser, J. Phys. Chem. B **114**, 7951 (2010).
[25]N. E. Levinger, R. Costard, E. T. J. Nibbering, and T. Elsaesser, J. Phys. Chem. A **115**, 11952 (2011).
[26]R. Costard, I. A. Heisler, and T. Elsaesser, J. Phys. Chem. Lett. **5**, 506 (2014).
[27]E. Steger and K. Herzog, Z. Anorg. Allg. Chem. **331**, 169 (1964).
[28]S. Brandán, S. Díaz, R. C. Picot, E. Disalvo, and A. B. Altabef, Spectrochim. Acta, Part A **66**, 1152 (2007).
[29]M. Klähn, G. Mathias, C. Kötting, M. Nonella, J. Schlitter, K. Gerwert, and P. Tavan, J. Phys. Chem. A **108**, 6186 (2004).
[30]J. VandeVondele, P. Tröster, P. Tavan, and G. Mathias, J. Phys. Chem. A **116**, 2466 (2012).
[31]H. R. Zelsmann, J. Mol. Struct. **350**, 95 (1995).
[32]See supplementary material at http://dx.doi.org/10.1063/1.4914152 for an analysis of the perturbed free induction decay, a comparison of structural fluctuations around $H_2PO_4^-$ and phospholipids, a method benchmark for calculations of vibrational frequencies, and further details about hydrogen bond dynamics derived from results of MD simulations.
[33]N. M. Levinson, E. E. Bolte, C. S. Miller, S. A. Corcelli, and S. G. Boxer, J. Am. Chem. Soc. **133**, 13236 (2011).
[34]P. E. Mason, J. M. Cruickshank, G. W. Neilson, and P. Buchanan, Phys. Chem. Chem. Phys. **5**, 4686 (2003).
[35]A. B. Pribil, T. S. Hofer, B. R. Randolf, and B. M. Rode, J. Comput. Chem. **29**, 2330 (2008).
[36]E. Tang, D. Di Tommaso, and N. H. de Leeuw, J. Chem. Phys. **130**, 234502 (2009).
[37]H.-S. Lee and M. E. Tuckerman, J. Chem. Phys. **126**, 164501 (2007).
[38]A. Bankura, V. Carnevale, and M. L. Klein, J. Chem. Phys. **138**, 014501 (2013).
[39]R. Kumar, J. R. Schmidt, and J. L. Skinner, J. Chem. Phys. **126**, 204107 (2007).
[40]O. Markovitch and N. Agmon, J. Chem. Phys. **129**, 084505 (2008).
[41]A. Luzar and D. Chandler, Nature **379**, 55 (1996).
[42]P. Hamm, Chem. Phys. **200**, 415 (1995).
[43]S. Mukamel, *Principles of Nonlinear Optical Spectroscopy*, Oxford Series on Optical and Imaging Sciences, 3rd ed. (Oxford University Press, USA, 1999).
[44]P. Hamm and M. Zanni, *Concepts and Methods of 2D Infrared Spectroscopy*, 1st ed. (Cambridge University Press, 2011).
[45]B. Auer, R. Kumar, J. R. Schmidt, and J. L. Skinner, Proc. Natl. Acad. Sci. U. S. A. **104**, 14215 (2007).
[46]J. D. Eaves, J. J. Loparo, C. J. Fecko, S. T. Roberts, A. Tokmakoff, and P. L. Geissler, Proc. Natl. Acad. Sci. U. S. A. **102**, 13019 (2005).
[47]M. Pasenkiewicz-Gierula, Y. Takaoka, H. Miyagawa, K. Kitamura, and A. Kusumi, J. Phys. Chem. A **101**, 3677 (1997).
[48]R. A. Kaindl, M. Wurm, K. Reimann, P. Hamm, A. M. Weiner, and M. Woerner, J. Opt. Soc. Am. B **17**, 2086 (2000).
[49]M. J. Tauber, R. A. Mathies, X. Chen, and S. E. Bradforth, Rev. Sci. Instrum. **74**, 4958 (2003).